UCRL 2474

UNIVERSITY OF CALIFORNIA

Radiation Laboratory

BERKELEY, CALIFORNIA

DISCLAIMER

UNIVERSITY OF CALIFORNIA
Radiation Laboratory

Cover Sheet
Do not remove

INDEX NO. UCRL-2474
This document contains 46 pages
This is copy 12 of 20 series A
Date FEB 8 1954

DECLASSIFIED

Issued to University of Calif.
Radiation Lab., Berkeley

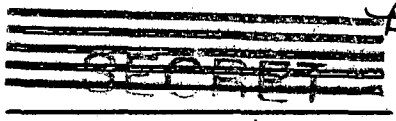

Classification

Each person who receives this document must sign the cover sheet in the space below.

Route to	Noted by	Date	Route to	Noted by	Date
B Moyer	BM				
W Latimer	WL				

RL-220

UCRL-2474
Materials Testing
Accelerator Distribution

UNIVERSITY OF CALIFORNIA

Radiation Laboratory

Contract No. W-7405-eng-48

MTA PROGRESS REPORT

June through November, 1953

February 8, 1954

Berkeley, California

Standard Distribution: Series A	Copy Number
Armed Forces Special Weapons Project, Washington	1
Atomic Energy Commission, Washington	2-3
California Research and Development Company	4-8
Patent Branch, Washington	9
San Francisco Operations Office	10
University of California Radiation Laboratory, Berkeley	11-15
Technical Information Service, Oak Ridge	16-20

Previous M. T. A. Quarterly Reports:

No. 1 UCRL-1009, March through August, 1950
No. 2 UCRL-1137, September through November, 1950
No. 3 UCRL-1297, December, 1950 through February, 1951
No. 4 UCRL-1436, March through May, 1951
No. 5 UCRL-1573, June through August, 1951
No. 6 UCRL-1680, September through November, 1951
No. 7 UCRL-1774, December, 1951 through February, 1952
No. 8 UCRL-1903, March through May, 1952
No. 9 UCRL-2043, June through August, 1952
No. 10 UCRL-2097, September through November, 1952
No. 11 UCRL-2194, December, 1952 through February, 1953
No. 12 UCRL-2318, March through May, 1953

INFORMATION DIVISION
Radiation Laboratory
University of California
Berkeley, California

MTA PROGRESS REPORT

June through November, 1953

TABLE OF CONTENTS

UCRL-2474

MTA PROGRESS REPORT

June through November, 1953

Radiation Laboratory, Department of Physics
University of California, Berkeley, California

February 8, 1954

I. INTRODUCTION

C. M. Van Atta

This report covers the contributions of UCRL to the MTA research and development program during the period June 1 to November 30, 1953. In this program UCRL continues to work in close collaboration with the California Research and Development Company (CRD).

Accelerator Development

During the past several months the problem of the optimum design for a high-current production accelerator has been under investigation. On the basis of available oscillator-tube (RCA A2332) performance the frequency of 49 Mc/sec has been selected as the highest frequency practicable without undertaking an expensive and time-consuming program of tube development. This choice of frequency would also appear to be acceptable in terms of production costs, since a study of MTA economics by CRD indicates that production costs decrease rapidly with increasing frequency from 12 to 50 Mc, but beyond 50 Mc decrease only very slowly. Thus there seems to be little economic incentive to strive for a higher frequency than that for which the RCA A2332 tube is effective.

At 49 Mc a resonant-cavity accelerator design for deuterons above about 4 Mev is straightforward, using the regular $\beta\lambda$ drift-tube geometry and solenoidal focusing. The difficult design problems lie in the means of accelerating deuterons from some convenient injection energy of 100–200 kev to that for which the $\beta\lambda$ geometry becomes feasible. The experimental effort of CRD is being directed toward an operational test of a preaccelerator configuration designated as "Ion III", consisting of a sequence of two or more quarter-wave-mounted drift tubes alternating with focusing magnets, the beam dynamics of which has been studied in some detail by the CRD theoretical group. An alternative preaccelerator configuration having attractive possibilities is a resonant cavity with 2 $\beta\lambda$ drift-tube geometry. In either case both magnetic alternating gradient (Brookhaven) and solenoidal focusing are feasible. Of the several drift-tube and focusing combinations under active consideration as the A-54 accelerator, the following are typical:

Alternative Configurations for the MTA A-54 Accelerator

Energies are stated for deuterons and are approximate.
D. C. injection at 200 kev.

A. G. F. = alternating-gradient focusing S. F. = solenoidal focusing

	(a)	(b)	(c)
1.	24.5 Mc Ion III with A. G. F. 0.2 to 1.0 Mev	49 Mc, $\beta\lambda$ with A. G. F. 1.0 to 6.5 Mev	49 Mc, $\beta\lambda$ with A. G. F. 6.5 to 13 Mev
2.	24.5 Mc Ion III with S. F. 0.2 to 1.0 Mev	49 Mc, 2 $\beta\lambda$ with S. F. 1.0 to 3.8 Mev	49 Mc, $\beta\lambda$ with S. F. 3.8 to 10 Mev
3.	49 Mc, 2 $\beta\lambda$ with A. G. F. 0.2 to 1.0 Mev	49 Mc, $\beta\lambda$, with A. G. F. 1.0 to 6.5 Mev	
4.	49 Mc, 2 $\beta\lambda$ with S. F. 0.2 to 1.0 Mev	49 Mc, 2 $\beta\lambda$ with S. F. 1.0 to 3.8 Mev	

Any of the above combinations can be built by utilizing two accelerator cavities, each twenty feet long. The velocity at the output of any of the above combinations is great enough so that a resonant-cavity $\beta\lambda$ geometry with solenoidal focusing is easily feasible for extension to higher energies.

A critical study of the properties of alternating-gradient focusing systems as applied to linear accelerators has been carried out. This study has shown that, as compared with solenoidal focusing, an alternating-gradient focusing system is much more sensitively dependent upon adjustment of the local focusing fields and upon mechanical alignment. In a high-current accelerator, in which loss of beam may cause damage to the machine, these disadvantages of alternating-gradient focusing systems are judged to be sufficiently serious that a solenoidal system should be used if possible. Recent studies have shown that configurations 2 and 4, utilizing solenoidal focusing throughout, are feasible without excessive focusing-magnet power and are therefore favored over configurations 1 and 3, utilizing alternating-gradient focusing.

Testing of the high-frequency power output of the latest model RCA A2332 tube with a ceramic envelope has continued at 49 megacycles/second. After a sequence of circuit improvements it was found that continuous high-frequency power output of about 600 kw could be sustained indefinitely. However, a brief period of operation at 650 kw resulted in a gradual loss of emission. Whereas the 600-kw output already demonstrated is sufficient for application of the A2332 to a production MTA, it is believed that by more vigorous degassing of the tube elements before sealing off from the pumps, and with some minor modifications, RCA will be able to produce tubes of the A2332 type capable of significantly greater high-frequency power output at 49 Mc.

Target Research

The major goals for the target research program are the determination of neutron yield as a function of deuteron and proton energy and the measurement of nuclear cross sections involved in the process of neutron production.

The method previously described of producing 320-Mev deuterons by stripping 500-Mev He^3 particles has been optimized. The He^3 gas-circulating and recovery system has been fully engineered and installed as a regular accessory to the 184-inch cyclotron. The energy distribution of the 320-Mev stripped deuteron beam has been studied by both time-of-flight and attenuation-curve methods.

Inelastic cross sections for high-energy protons, deuterons and α-particles and the deuteron stripping cross section have been measured. From these results an empirical relationship has been developed for the dependence of inelastic cross sections upon type of bombarding particle and target nucleus. The effect of the new cross sections upon neutron-yield calculations is briefly discussed.

The large liquid scintillator, which should give much more detailed information about the processes involved in neutron production, is nearing completion. The goal is to observe directly the number of neutrons per individual nuclear event. Also, a counter telescope utilizing recoil protons from n-p scattering is being developed for determining the number of neutrons per second in a high-energy neutron beam. By monitoring the neutron beam with this device and measuring the yield of evaporation neutrons produced by the beam incident on various targets by the water-tank method, the number of evaporation neutrons per incident high-energy neutron (90, 160 and 270 Mev) can be determined.

Rapid progress is being made on the conversion of the 184-inch cyclotron for higher energies (456-Mev deuterons, 730-Mev protons, 1140-Mev He^3 from which 720-Mev stripped deuterons can be produced). This work is reported in detail in the UCRL physics monthly and quarterly progress reports. Shutdown for conversion is scheduled to occur about April 5, 1954. In the meantime, an effort will be made to complete all measurements pertinent to the MTA at the energies now available before the shutdown date.

II. ACCELERATOR DEVELOPMENT

Beam Dynamics Studies

Fred N. Holmquist, Jr., Henry P. Kramer, and Lloyd Smith

At the beginning of this period a differential-analyzer study was made of an accelerator with the following characteristics:

Type	2 $\beta\lambda$
Frequency	43.5 Mc
Bore	4 in. diameter
Injection	100-kv deuterons
Voltage gradient	0.15 Mv/ft
Synchronous phase	60°

Focusing was accomplished by quadrupole magnets. The interest in this case arises from the fact that the transit-time factors for on-axis particles run as low as 0.08. The on-axis phase acceptance was about 180°, as expected, but off-axis acceptance was considerably worse, and even the surviving trajectories showed sudden and somewhat alarming fluctuations. These results, combined with earlier experience, have led us to the working principle that accelerators with small relative velocity change per gap, on-axis transit time factors of about 0.20 or greater, voltage gradients not exceeding the limits set in UCRL-2203, and strong-focusing magnetic lenses will show on a differential analyzer "normal" behavior; that is

Phase acceptance:	$3\phi_s$ (independent of radial displacement)
Radial acceptance:	$\pm (4/5)a$ entering focusing plane
	$\pm (2/5)a$ entering defocusing plane
Angular acceptance:	$\pm (3/5)(a/L)$ radians entering focusing plane
	$\pm (6/5)(a/L)$ radians entering defocusing plane

where

ϕ_s = synchronous phase
a = bore radius
L = repeat length of first strong-focusing elements.

Subsequently, two designs were made up which represented our best recommendations for actual construction. One was a $3/2$-$\beta\lambda$, 24.5-Mc, 3-in.-bore preaccelerator, which was not adopted because of its approximate similarity to the Ion III preaccelerator. The other, a 2-$\beta\lambda$, 49-Mc, 3-in.-bore preaccelerator, described in detail in UCRL-2350, was adopted. With minor changes in synchronous phase and g/L values to suit the vacuum tank that had been designed, it now constitutes one alternative for the first half of the accelerator designated as A-54. The differential analyzer was applied to both designs, but revealed nothing incompatible with the rules of thumb mentioned at the beginning of this section.

In order to get some idea of the actual appearance of the fields in the quadrupole magnets, a three-dimensional electrolytic tank model of the pole pieces was made and potentials were measured in the plane through the pole tip. Such a measurement, plus the assumptions that the potential varies in azimuth as sin 2ϕ and that saturation is unimportant, is sufficient to determine all three field components everywhere. It was found that the transverse components of the fields, even in the first magnets, should be quite linear in their dependence on transverse displacement. A tentative value for the magnetic fields at the bore radius at the axial center of the magnets was obtained by using the differential analyzer to map out the stability diagram for the measured axial dependence of the fields, and then choosing the field appropriate to the center of the stability diagram for the on-axis synchronous particle. Work is still in progress to determine the effect of the measured axial field components on the beam.

A study was made of the effects of various sorts of misalignments of drift tubes on particle motion in the strong-focusing field. The most important result can be stated in the form of a formula: If the magnetic center lines of the magnets deviate from a common straight line in a random way, an oscillation is induced which adds to the normal oscillations. The most probable value of the extra displacement is given by:

$$\Delta X \sim 4\sqrt{N}\,\delta$$

where δ = r.m.s. value of individual misalignments
N = number of drift tubes.

The numerical factor is determined primarily by position in the strong-focusing stability diagram and measures the amplitude induced by a single misalignment.

This extra displacement effectively cuts down the geometrical area of the bore by a factor $[1 - (\Delta X/a)]^2$, and one can only assume at this stage that the beam would be decreased by the same factor. The conclusion is that considerable care is needed in lining up the magnetic centers; and while it seems possible to do so for short accelerators such as A-54, it might prove a formidable obstacle for a production machine. This objection served to re-emphasize other unattractive properties of strong-focusing systems, in particular that, for an entering beam of small angular divergence, much of the geometrical area of the bore is wasted, and that the failure of one magnet would seriously hamper operation.

A new study of solenoidal focusing led to the conclusion that solenoids could be used, possibly with some sacrifice in output energy of A-54 due to the need of reducing the radial defocusing forces. The output energy of the two tanks would be reduced from 6.5 Mev to not less than 3.8 Mev, but the exact figures wait on power and field tests of some solenoids. A tentative decision has been made to design the drift tubes to accomodate either type of focusing system, but to try the solenoids first. A more detailed account of the comparative features of the two systems is given in LWS-30012 by Moore, Hiskes and Vetterlein. Judging from the detailed studies of strong-focusing accelerators and the earlier studies of A-12, there is no reason to believe that solenoidal focusing adapted to A-54 would introduce any harmful anomalies in the trajectory patterns.

In connection with the efforts to set up the orbit equations for an electronic computer, empirical formulas have been developed that should adequately represent the radial and axial electric fields in drift-tube gaps for the range of gap-to-bore ratios covered in A-54. The establishment of such a computing program is being actively pursued by CRD.

Magnet Design Studies

Edward L. Hubbard

In a linear accelerator with strong-focusing magnets inside the drift tubes the focusing field strengths required increase as the low-energy end of the machine is approached. At the same time the space available for the magnets and the gaps between magnets is reduced. As a result the minimum injection energy is limited by the maximum focusing fields that can be obtained.

To avoid excessive power dissipation in the magnet windings, it is desirable to operate with the flux densities in the poles and yoke below the saturation value. The large leakage fluxes produce flux densities in the iron that are two to four times the maximum field inside the bore tube. Since the leakage fluxes are difficult to predict, several full-scale model magnets have been built to determine the maximum focusing fields that are practical.

A. Model Design and Test Methods

The first three models consisted of just one pole and a quarter section of the yoke. During the tests these models were placed between steel plates that were located in the planes of zero magnetic potential that exist in a sequence of full 4-pole magnets. Fig. 1 is a drawing of a typical pole and quarter section of yoke and shows the symbols for the dimensions that will be used below. When a preliminary design for A-54 was chosen, a full 4-pole magnet for the first drift tube of the first 1 $\beta\lambda$ tank (magnet No. X1) was constructed and tested with large sheets of steel fixing the planes of zero magnetic potential that would exist between it and the adjacent magnets of the machine.

Before the coil was mounted on the pole piece, several loops of small wire were wound around the pole at various positions. To determine the flux densities at these positions in the pole, the flux through these loops was measured with a fluxmeter when the current in the coil was pulsed on and off. The focusing magnetic fields were measured with a small coil or a bismuth wire probe placed against the center of the pole tip.

To minimize the leakage flux between adjacent poles of the same magnet the width of the pole tip w_T should be as small as possible. Electrolytic tank measurements[1] indicate that w_T can be made as small as 1.3a without excessive distortion of the hyperbolic fields inside a circular aperture of radius a. They also show that the fields in this region are satisfactory if the hyperbolic surfaces are replaced with circular ones of radius R = 1.09a. These

1 E. L. Hubbard and C. S. Nunan, UCRL Engineering Note, 4111-63:03.

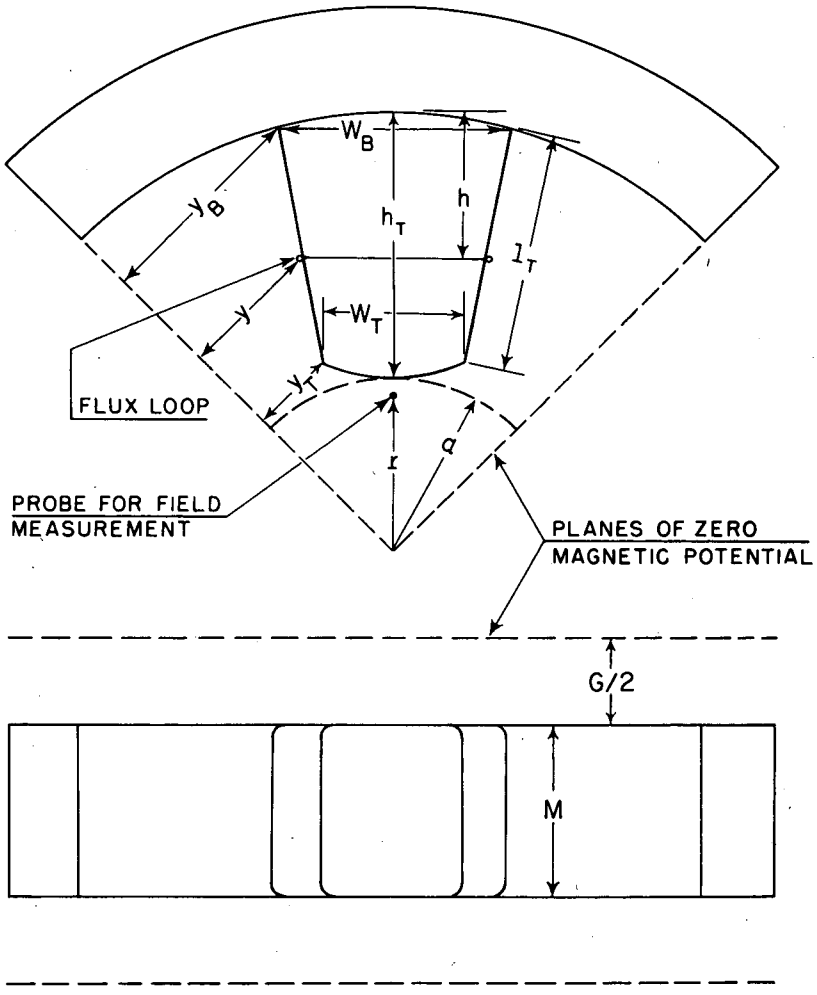

MAGNET DESIGN STUDIES.

MU-7145

Sec. II, Fig. 1 Typical pole and quarter section of yoke.

choices of w_T and R were used in designing the model magnets, although owing to saturation effects in the iron the magnetic fields may have a shape different from the fields of the electrolytic tank. Experimental mapping of the magnetic fields is being planned, and if the distortion of the fields turns out to be appreciable, it can be corrected by shimming at a later time.

To minimize the leakage flux the coils were wound around the pole on all the models. The electrolytic tank measurements and beam dynamics indicate that it is desirable to make the length of the pole M at least half the repeat length. This choice of M severely limits the space available between the pole and the drift-tube skin for the coil. Therefore it is necessary to use a high current density in the coils and to cool them with high-pressure water.

The model magnets were designed to reduce the flux density at the base of the pole as much as possible by making the pole short and using high current densities or by tapering the pole to make the width of the base w_B larger than the width of the tip w_T.

The poles have been made of ordinary mild steel, which saturates at about 20,000 gauss. The only materials that saturate at appreciably higher flux densities are cobalt alloys that saturate at 24,000 gauss. They were not used because they are difficult to machine, are expensive, and are not readily available in large sizes.

B. Model Results

(1) Bevatron Magnets. While the first models were being designed, measurements were made on the magnets that were built to focus the output beam of the linear accelerator that will inject into the bevatron.[2] The shape of the poles used in these magnets and the positions of the flux loops are shown in Fig. 2. The magnetization curve for the focusing fields and the flux densities in the pole pieces are shown in Fig. 3. The curves shown in Fig. 3 are for the center magnet in a sequence of three. Because of the large air-cooled coils, the spacing between magnets was so large that there was little difference between the measurements with three coils and with one coil by itself.

(2) Model I. The shape of the pole for Model I is shown in Fig. 4. It was designed so that the gap between the tapered sections of adjacent poles of the same magnet would be equal to the gap between adjacent magnets. The data in Fig. 5 show that the large taper allowed a focusing field of 9000 gauss at the pole tip with a flux density of only 16,000 gauss in loop 3 at the base of the pole, but that saturation of the iron near loop 2 at the neck of the pole caused the magnetization curve to level off.

The coil for Model I had taps so that current could be put through only part of the winding. When the part nearest the pole tip was used, the data were nearly the same as those shown in Fig. 5.

(3) Model II. Since tapered poles like the one in Model I are difficult to make, Model II was designed with a short straight pole to see what fields could be obtained without the taper. The data are given in Figs. 6 and

---

2 Bruce Cork and Emery Zajec, UCRL-2182.

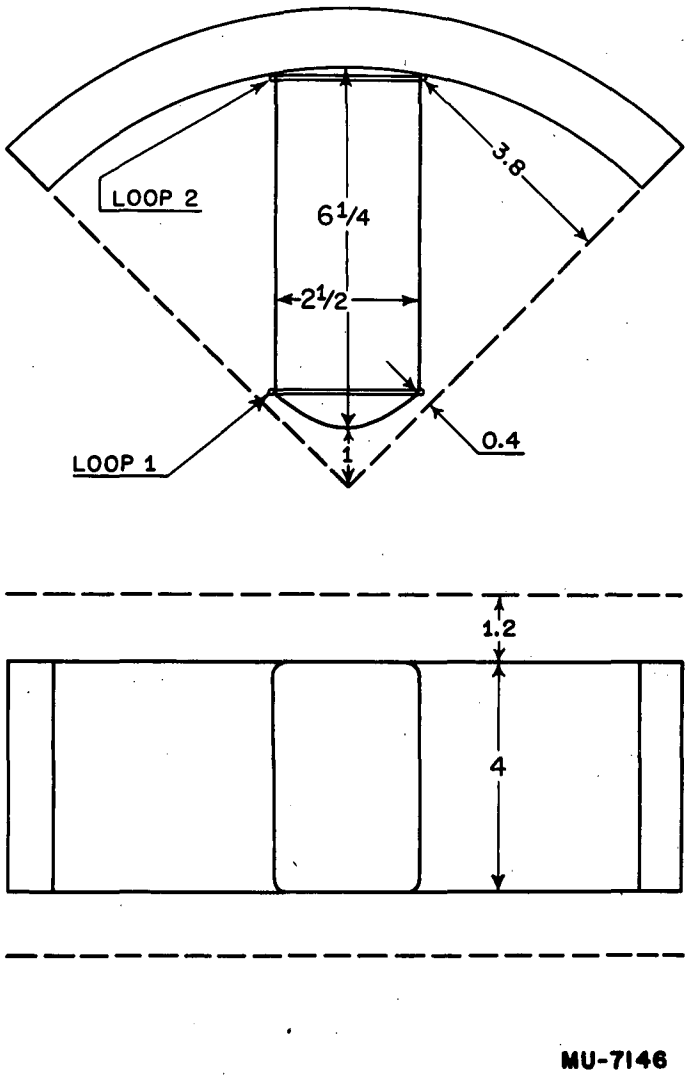

Sec. II, Fig. 2 Pole of magnets for bevatron injector.

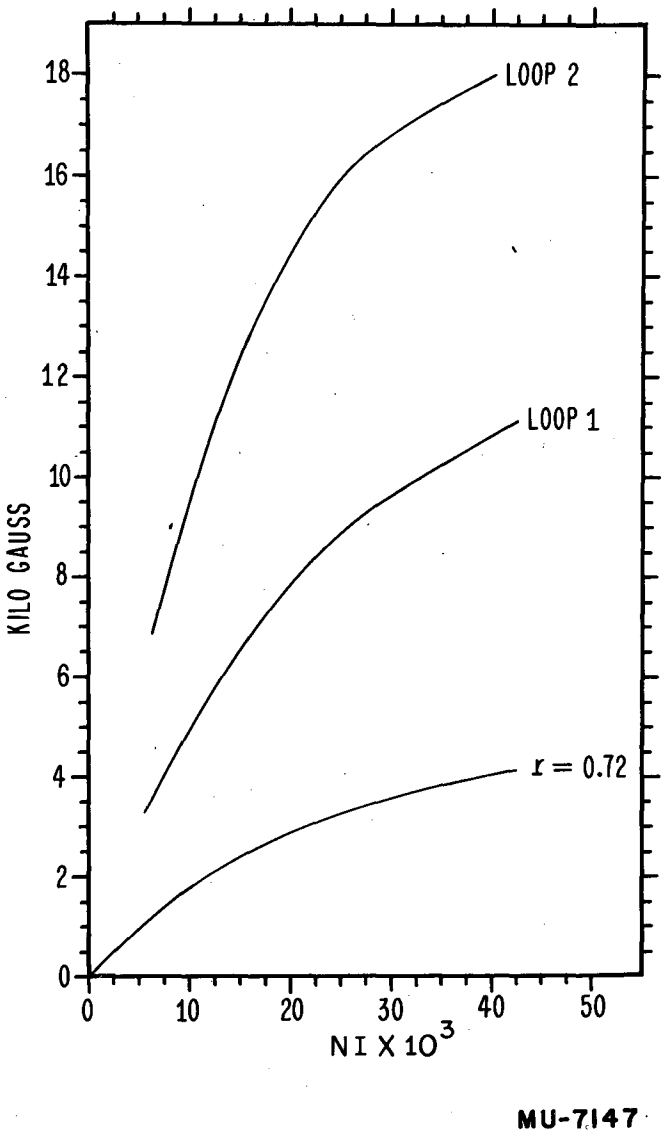

Sec. II, Fig. 3 Magnetic measurement data for bevatron magnets. The position of the flux loops is shown in Fig. 2; r is the distance from the axis of the magnets to the center of the probe that was used to measure the focusing magnetic field.

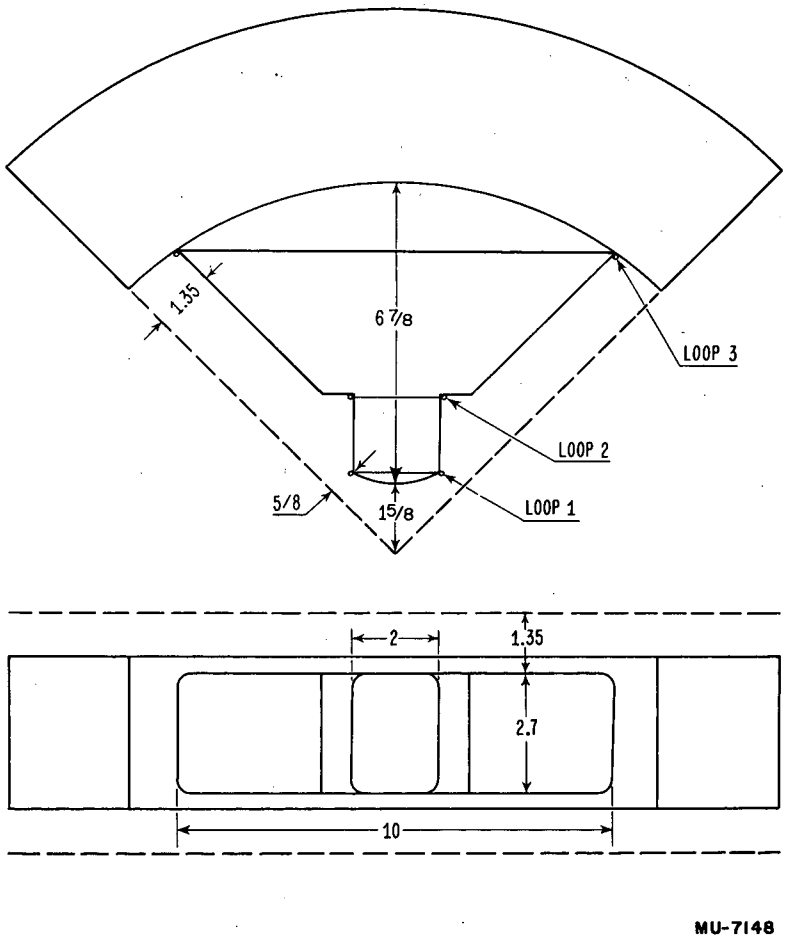

Sec. II, Fig. 4 Model I pole.

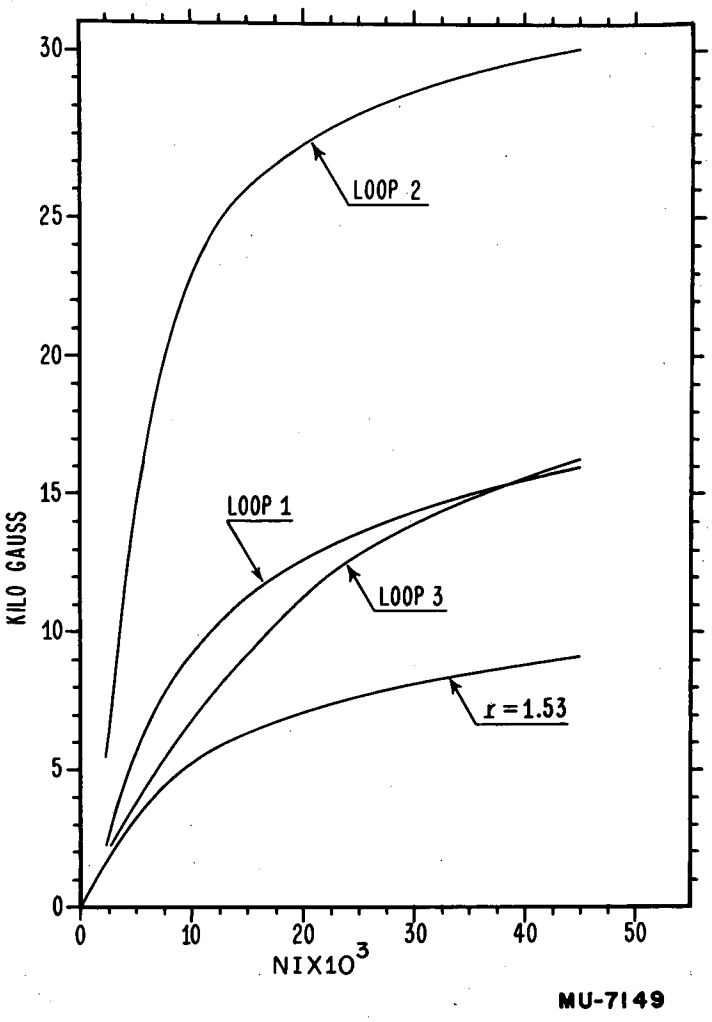

Sec. II, Fig. 5 Magnetic measurements on Model I.

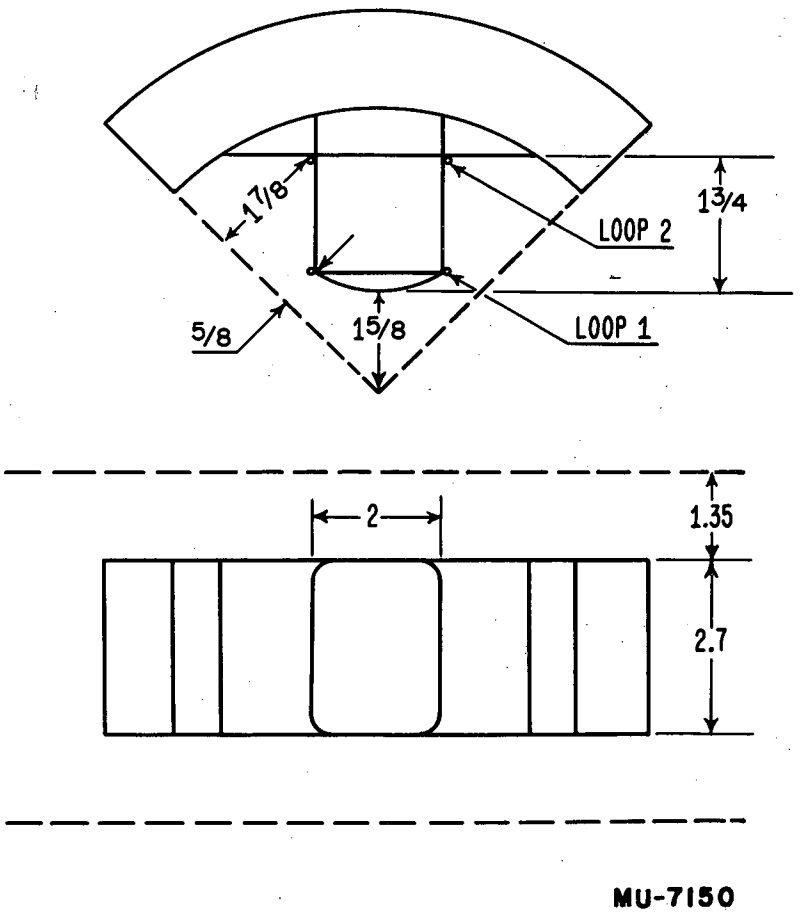

Sec. II, Fig. 6 Model II pole.

7. Model II was also tested with one of the gaps between the pole and the ground plane reduced to 0.8 in. The results of the measurements were not much different from those shown in Fig. 7.

(4) Model III. The results from Models I and II indicated that the best ratio of focusing-field strength to maximum flux density in the pole piece would be obtained with a short pole that was tapered all the way down to the tip. The shape of the pole for Model III is shown in Fig. 8. It is designed for a drift tube with a four-inch bore. The data in Fig. 9 show that the maximum flux density was in the center of the pole rather than at the base.

(5) Model X1. The choice of a three-inch bore and the field requirement of 7200 gauss at a radius of 1.625 in. for magnet No. X1 made it possible to use a smaller taper, a longer pole, and a lower current density than in Model III. The pole shape chosen is shown in Fig. 10 and the data in Fig. 11.

The mechanical design of the single-pole magnets was done by Robert Young (UCRL) and the mechanical design of the Model X1 magnet by Forrest Parry (CRD). The magnetic measurements were carried out by the magnetic measurements group at UCRL under the direction of Harry Keller.

C. Design Equations

When the iron in the pole is not saturated, the reluctance of the iron in the magnetic circuit can be neglected, and the number of ampere-turns required per pole can be calculated from

$$NI = 1.01\, aH \qquad (1)$$

where H is the focusing magnetic field at the radius a at the center of the pole tip. H is in gauss, I in amperes, and a in inches. When part of the pole reaches saturation, the number of ampere-turns given by equation (1) can be corrected by multiplying by a factor of 1/E. The values of E obtained with the models are shown in Fig. 12 as a function of the maximum flux density in the pole. Some difference between the curves for the different models is to be expected, since E depends on the way in which the flux density varies with the position in the pole piece as well as on the maximum value. Also the steel used in the different models may have had different magnetic properties. The faster decrease of E with high flux densities for Model X1 is probably due to the high flux densities of about 19,000 gauss in the yoke of the magnet.

To predict the flux densities in the poles, some approximate semi-empirical equations have been developed for poles with the simple shape shown in Fig. 1. The flux densities calculated from them agree with the model measurements to within 10 percent. The notation used in these equations is the same as that in Fig. 1. The flux that enters the pole through the circular (or hyperbolic) surface at the pole tip is given by

$$\phi_T = Hw_T(M + a)\left[1 + \left(\frac{w_T^2}{4a^2}\right)\right]^{1/2} . \qquad (2)$$

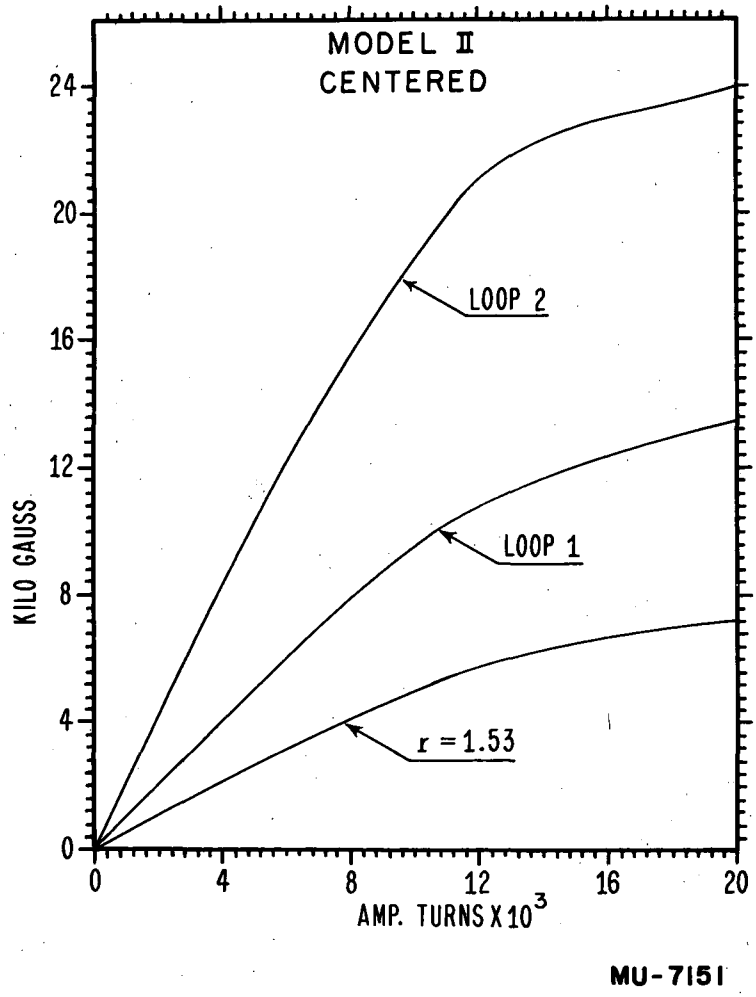

Sec. II, Fig. 7 Magnetic measurements on Model II.

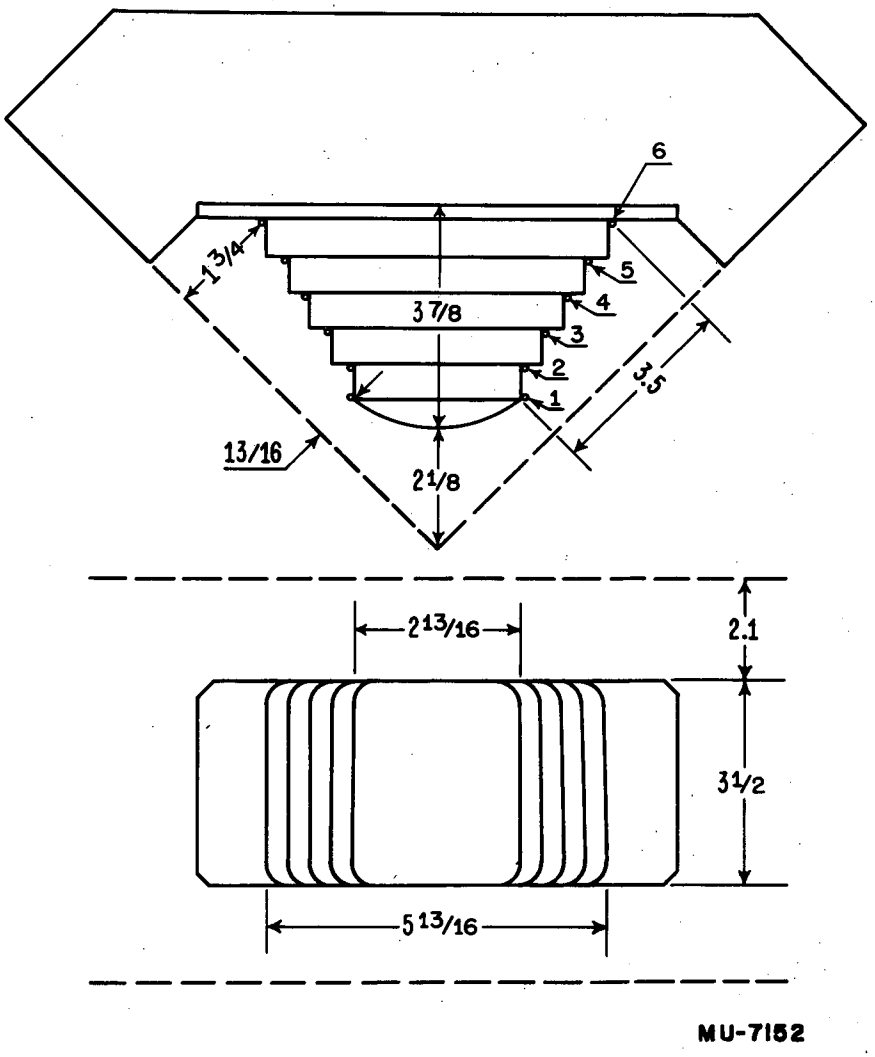

Sec. II, Fig. 8 Model III pole.

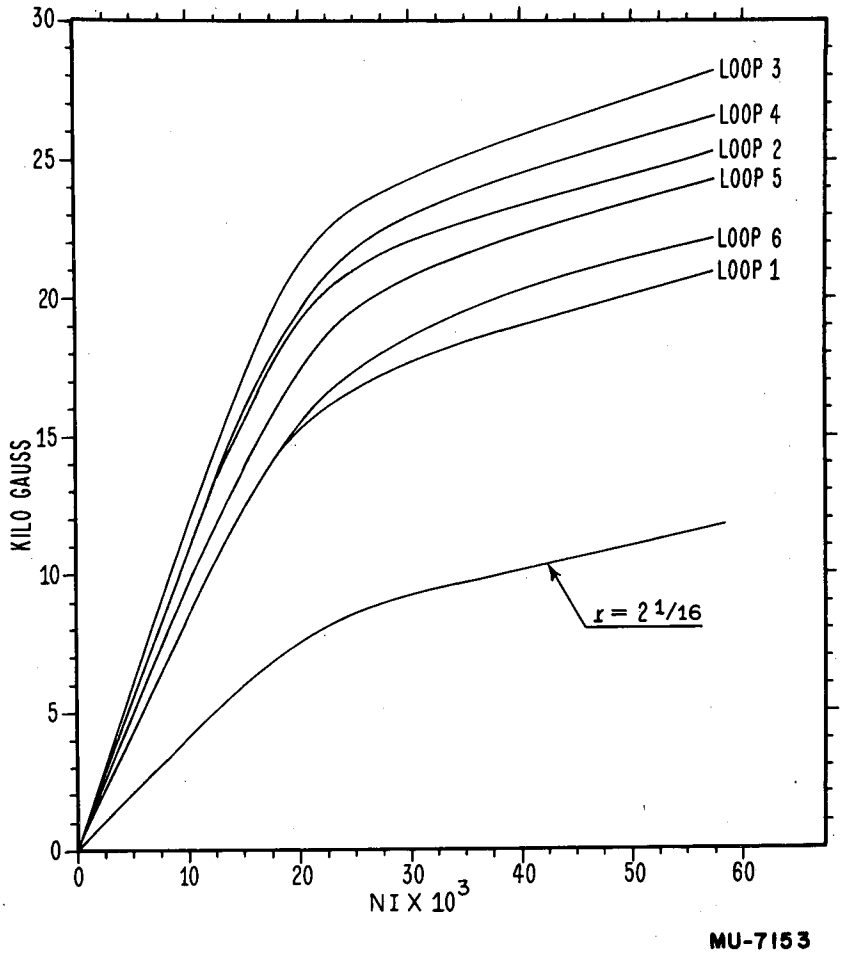

Sec. II, Fig. 9 Magnetic measurements on Model III.

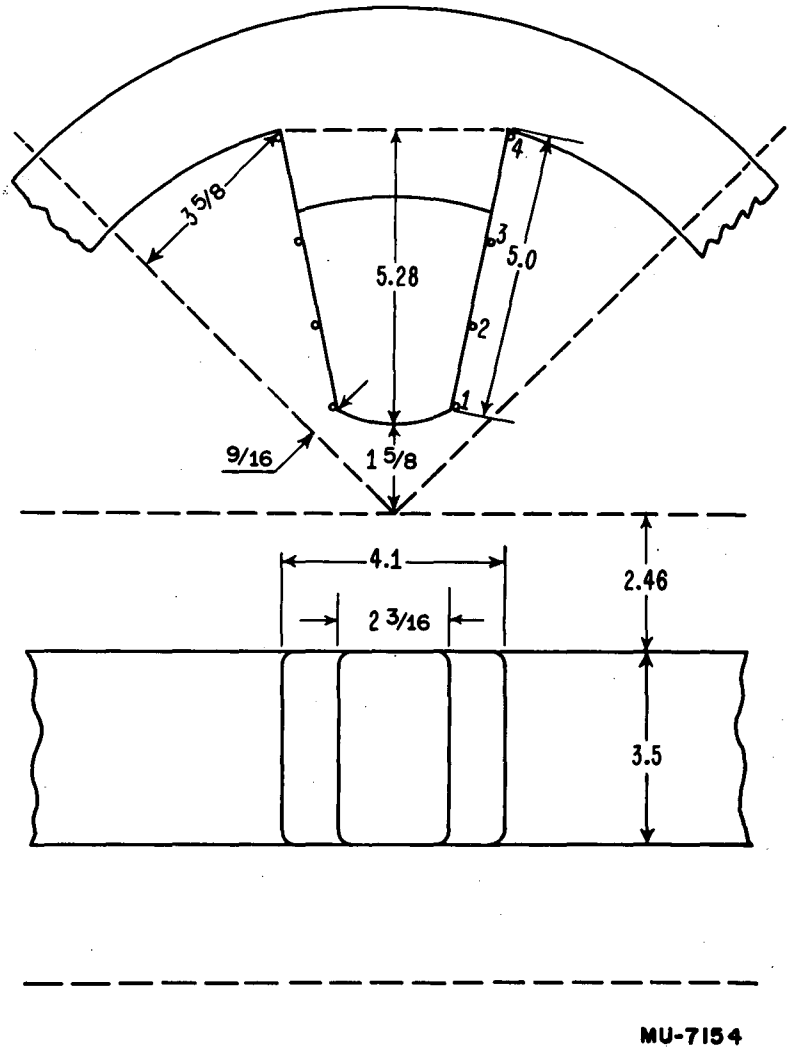

Sec. II, Fig. 10 Pole of Model XI magnet.

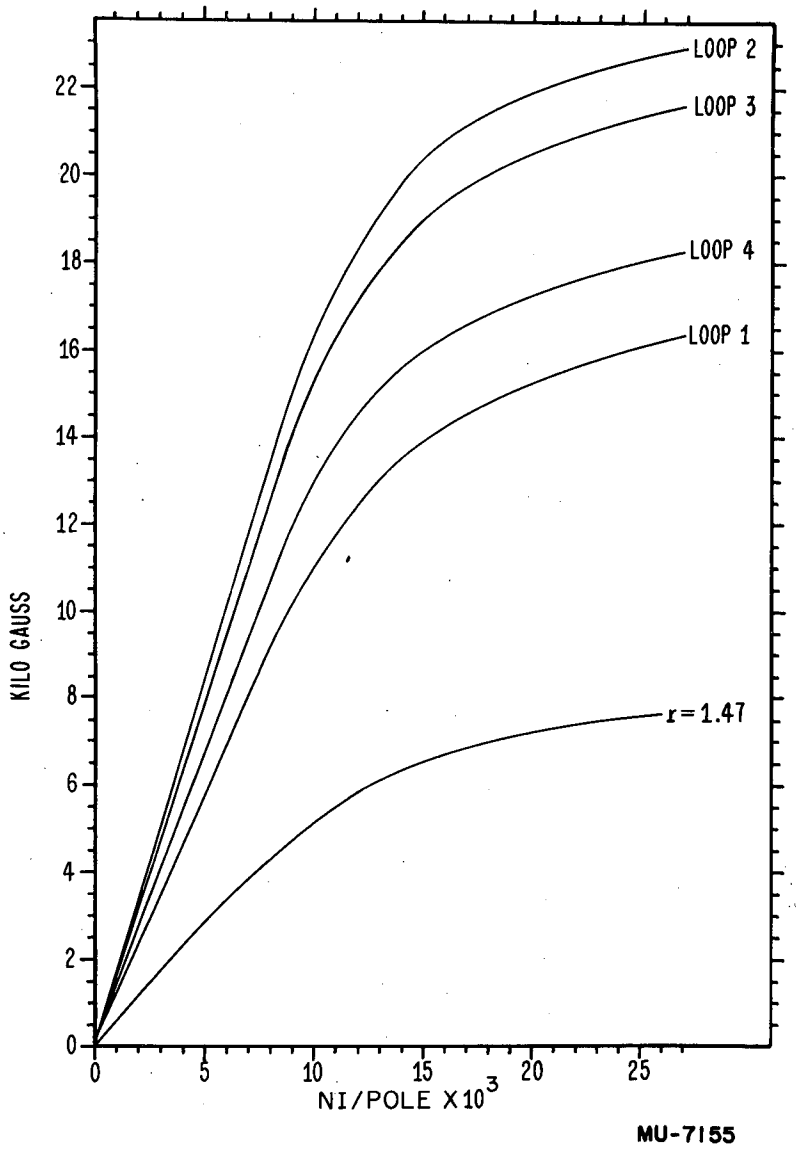

Sec. II, Fig. 11 Magnetic measurements on Model XI.

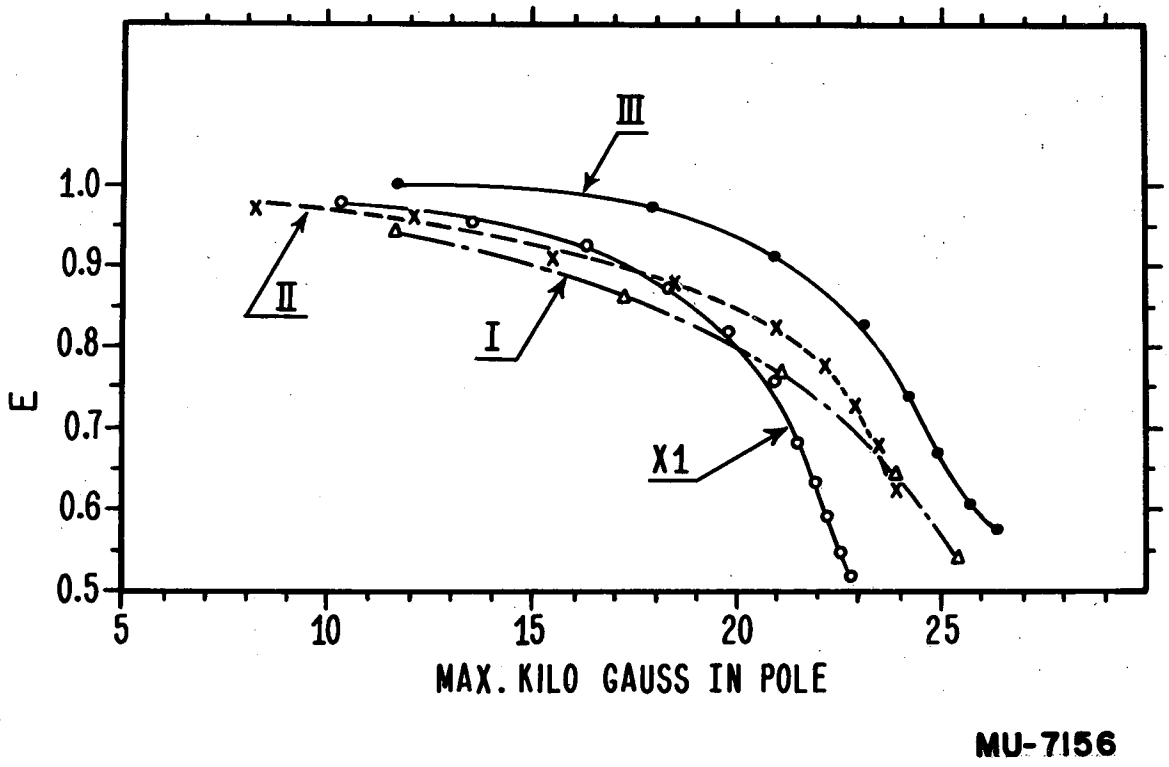

Sec. II, Fig. 12 Correction factor E to be applied to equation (1) for the model magnets.

The flux that goes through a flux loop at a distance h from the pole base consists of ϕ_T plus the leakage flux that enters the "end" surfaces of the pole that face the adjacent magnets and "side" surfaces that face the adjacent poles of the same magnet. The flux that enters one end surface between the tip and a flux loop at a distance h from the pole base is

$$\phi_E = \frac{a(h_T + G/4)H}{G}\left[\frac{w_B'}{6} + \frac{w_T'}{3} - \frac{w_B'}{2}\frac{h^2}{h_T^2} + \frac{1}{3}(w_B - w_T)\frac{h^3}{h_T^3}\right] \qquad (3)$$

where G = gap between magnets
$w_B' = w_B + G/2$
$w_T' = w_T + G/2$.

The flux that enters one side surface between the tip and the flux loop is

$$\phi_S = \frac{a(M + y_T)\ell_T H}{4y_B}\left\{1 + \frac{2}{3}\left(1 - \frac{y_T}{y_B}\right) - \left[1 + \frac{2}{3}\left(1 - \frac{y}{y_B}\right)\right]\frac{h^2}{h_T^2}\right\} \qquad (4)$$

If the gap G is the same on both sides of the magnet, the total flux through the flux loop is

$$\phi = \phi_T + 2\phi_E + 2\phi_S . \qquad (5)$$

D. Location of the Magnetic Axis

All components of the focusing magnetic field would be zero on the geometric axis of an ideal magnet. In practice, however, it is conceivable that at high flux densities, inhomogeneities in the pole material or irregularities in the windings might cause the magnetic axis to differ slightly from the geometric axis of the magnets. Calculations indicate that misalignments of the order of 1/32 in. in the magnetic axes of the drift tubes in the A-54 accelerator would result in a serious displacement of the beam.

A device has been developed that can be used for finding the magnetic axis of a magnet and for lining up the magnetic axes in the accelerator. A schematic drawing of this device is shown in Fig. 13. A cylindrical iron bob is mounted on a nonmagnetic wire spring. When the device is placed in the magnetic field with its axis parallel to the axis of the magnet, the bob is deflected by the magnetic field until the restoring force of the sptring becomes equal to the magnetic force. The spring constant is varied by adjusting the length of the spring with the slider.

The position of the magnetic axis of a magnet can be determined by moving the device until there is no deflection of the bob. Preliminary measurements on the Model X1 magnet indicate that inside the magnet, the magnetic axis is located on the geometrical axis to within the 10-mil accuracy to which the position of the geometric axis was determined. No particular care was used in positioning the coils on the magnet for these measurements. When the device was moved 10 mils off the magnetic axis, the bob was deflected about

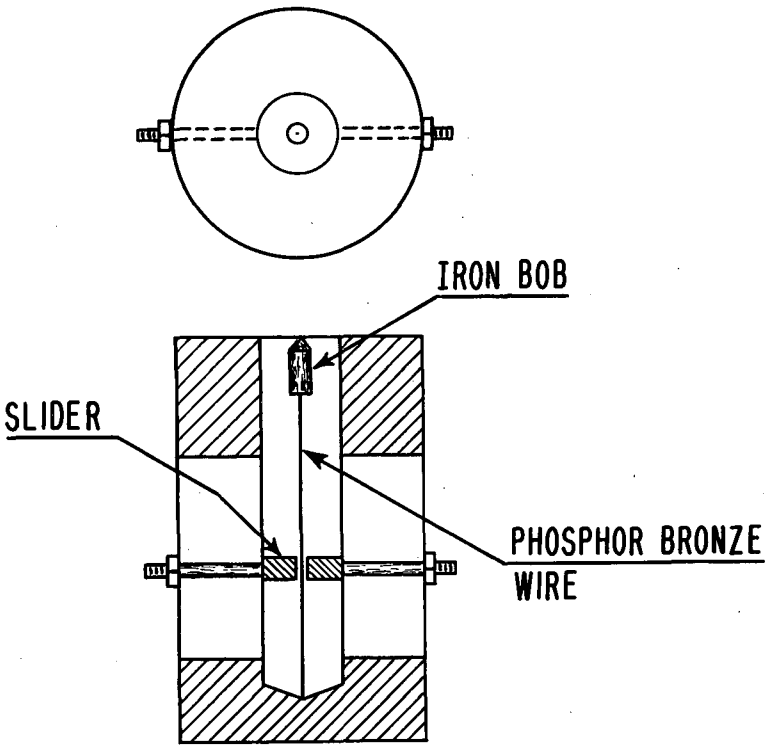

Sec. II, Fig. 13 Device for locating magnetic center of strong-focusing magnets.

1/16 in. In this position the magnetic axis could be shifted enough to center the bob again by shunting 7 percent of the current in the coil around one of the poles.

For lining up the magnetic axis of the accelerator, the device can be placed on the geometrical axis of the machine and the magnetic axis of the drift tubes moved until no deflection of the bob is obtained.

High-Frequency Program

William R. Baker

The RCA A2332 tube-testing program at UCRL has now progressed to a point at which it seems reasonably certain that the A-54 program can be assured of at least 600-kw CW at 20 kv and somewhat more than this at higher voltages. Operation has been primarily at 49 megacycles, but enough has been done at other points around this region to say that there is no particular frequency to avoid.

Two samples of the new ceramic-envelope tube have been operated over a period of several weeks. The first, 40 LFC, was limited in power by a faulty grid condition of a mechanical nature to a maximum of 500 kw. This trouble, however, was known to exist at RCA and the main value of operating it here was to check the ceramic envelope and copper seals at high frequency. These proved to be very good. No flashover trouble was experienced during any of the runs, many of which went to 22 kv, and the ceramic was never more than mildly warm to the touch nor the copper seals hot in spite of the high-frequency currents of over a thousand amperes that they were conducting during normal operation.

During one of these runs, however, a considerable amount of second harmonic (brought about by a circuit condition) did make the ceramic envelope dangerously hot. This points out the importance of avoiding circuit arrangements that allow such harmonic troubles to exist. In fact, there is at present a growing belief that it may be necessary to make use of the general scheme, described in detail in a previous report of this series, for reflecting zero impedance for the harmonics at the tube elements.

The second ceramic envelope tube did not suffer from the grid trouble associated with the first tube. It also appears to operate quietly without flashovers or envelope and seal-heating troubles. Its power output is considerably in excess of the earlier tube but has not as yet come up to the megawatt level expected. Just why is not yet understood fully, and is the subject of an investigation going on at the present time. This limiting feature is something which comes in after a period of a half hour or so of operation at a level of around 650 kw at 20 kv or at a slightly higher level at a higher voltage. The d-c grid voltage starts to fall rather slowly at first and then at a faster rate until the efficiency of the tube has dropped to around 65 percent. Measurements made while operating during this condition show it is not due to grid emission but somehow associated with a drop in cathode emission. The only theory so far advanced to explain the effect is that it is due to positive-ion bombardment of the cathode. The tube was not well processed at RCA and the trouble may

clear up with continued operation. Also, the low-frequency processing at RCA is probably not sufficient to get the gas out of the elements to the extent needed for our high-frequency service. Calculations show that ions formed at the anode by electron bombardment strike the cathode with essentially the full d-c voltage applied to the plate of the tube at our frequency, whereas at the lower frequencies used at RCA and in the previous MTA accelerator work the ion energy approaches the much lower value corresponding to the minimum plate voltage swing. There is a feeling that harmonic energy may contribute to this effect. We are at present working on this problem also.

Mechanical Design and Studies

William M. Brobeck

During this period an average of 2.4 members of the Mechanical Engineering Department were engaged in MTA work other than the 184-inch cyclotron modification. Their work consisted of liaison with CRD on the Mark I operational and experimental program, review of the CRD program and designs for the A-54 accelerator, and design work and studies on the MTA program--primarily related to the A-54 requirements. This time was distributed substantially as follows:

1.	Mark I Liaison	5 percent
2.	Tube Testing and Oscillator Development	67 percent
3.	Design Review and Preliminary Studies	28 percent

III. TARGET RESEARCH

The Production of 320-Mev Deuterons by He^3 Stripping

John Ise, Jr. and Robert V. Pyle, UCRL
and
Donald A. Hicks, CRD

Further attempts have been made to increase the external deuteron current (5×10^{-13} ampere from 95 percent enriched He^3) obtained by stripping 510-Mev He^3 nuclei inside the cyclotron. The position of the cyclotron source and the material, thickness, and position of the stripping target have been varied with no improvement. The He^3 recovery system (Fig. 1) has operated well, with the loss of 95 percent enriched He^3 (from all causes) of 0.8 cc per hour of running time.

The intensity distribution of stripped deuterons inside the cyclotron tank was measured with a cylindrical ionization chamber mounted vertically behind a lead collimator that could be rotated around the chamber (see Fig. 2). The chamber had a diameter of one inch and an active length of 5 inches and was surrounded by a brass shield of sufficient thickness to stop the He^3 ions and stripped protons but still thin enough to permit the stripped deuterons to enter the chamber. The lead collimator was 19 inches long with walls thick enough so that the only way ions could reach the chamber was down a 1-inch-wide channel. The apparatus was mounted on the proton probe and could be run into the cyclotron at various radii.

Rotation of the collimator presented some difficulties. Since the apparatus had to be moved in a vacuum and in a strong magnetic field, a commercial motor could not be used. A direct-current motor device was designed to use the magnetic field of the cyclotron, and was fabricated entirely from nonmagnetic materials. The motor is capable of delivering approximately 50 lb-in. at 400 revolutions per minute when in a field of 15 kilogauss. The major problem in using the motor in the cyclotron was the excessive sparking at the brushes because of the low pressure. The large heating that resulted caused the brush-holder insulation (paper-based bakelite) to carbonize, giving rise to an electrical short circuit. This was remedied satisfactorily for the short running time involved in this experiment by replacing the insulation with mica.

To obtain the intensity profile, the apparatus was run in to a particular radius and the ionization chamber readings were taken as a function of collimator angle. The results of the experiment are shown in Fig. 3. The arrows at various radii are in the direction of the maximum beam intensity at these radii, and their lengths are proportional to these maximum intensities.

The results show that the external beam intensity could be more than doubled by displacing the deuteron tube twelve inches. Because of the expense involved, however, this intensity increase is considered insufficient to justify the alteration.

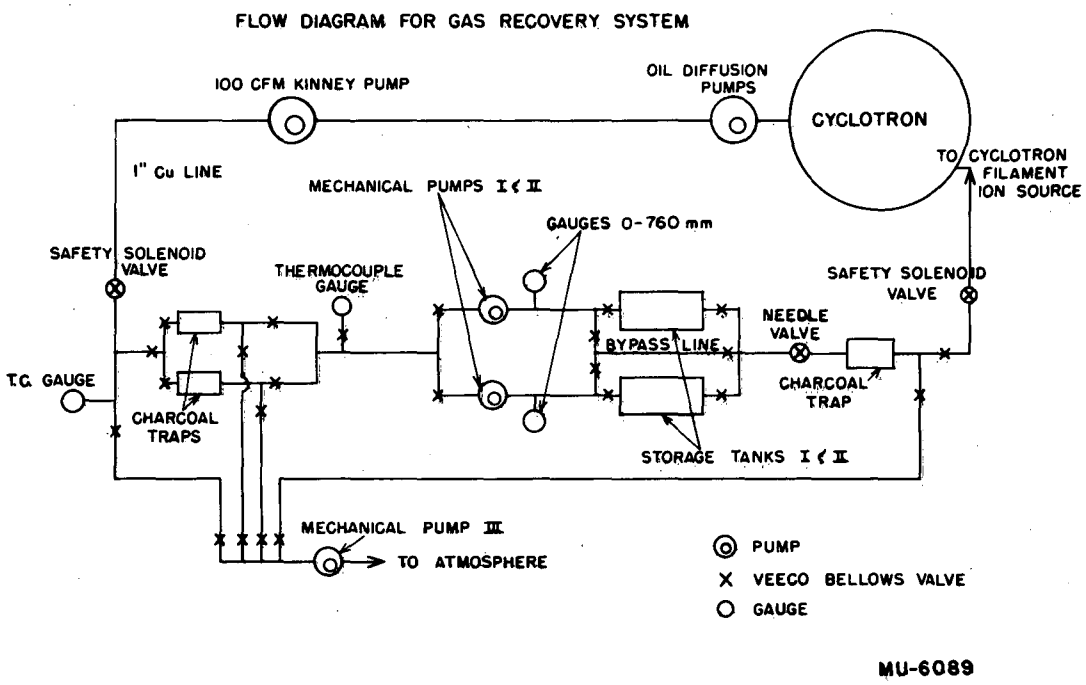

Sec. III, Fig. 1 Flow diagram for gas recovery system.

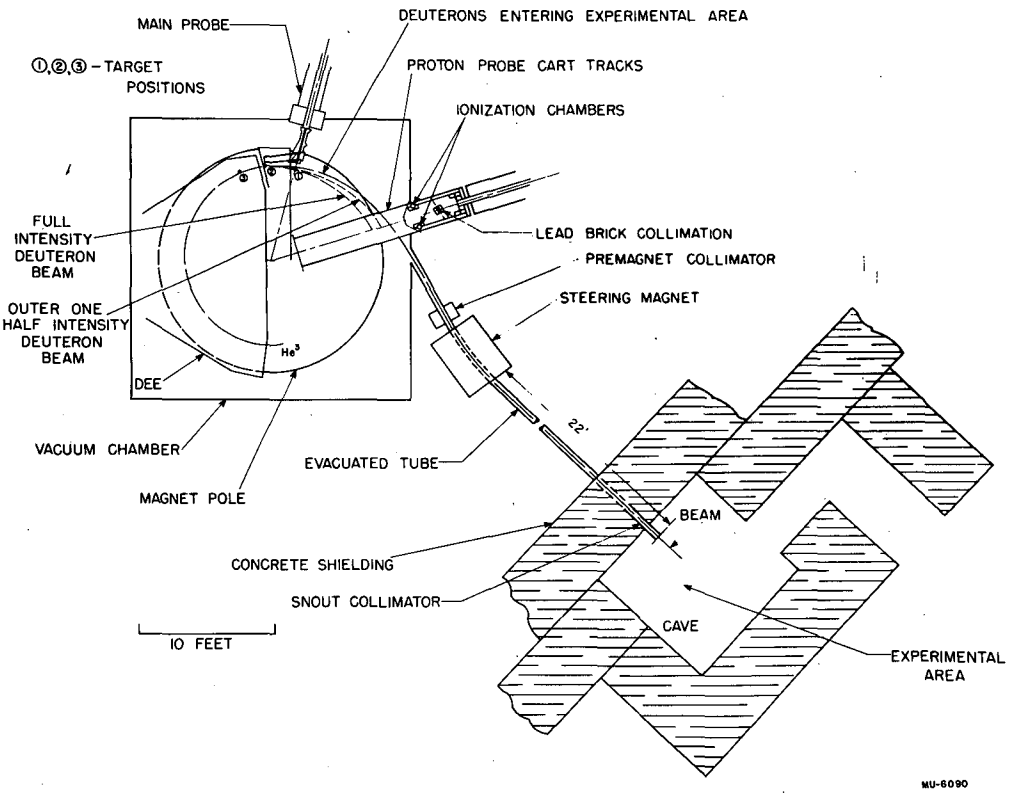
MAIN PROBE
DEUTERONS ENTERING EXPERIMENTAL AREA
①,②,③ – TARGET POSITIONS
PROTON PROBE CART TRACKS
IONIZATION CHAMBERS
FULL INTENSITY DEUTERON BEAM
LEAD BRICK COLLIMATION
PREMAGNET COLLIMATOR
STEERING MAGNET
OUTER ONE HALF INTENSITY DEUTERON BEAM
He^3
DEE
22'
VACUUM CHAMBER
EVACUATED TUBE
MAGNET POLE
BEAM
CONCRETE SHIELDING
SNOUT COLLIMATOR
CAVE
EXPERIMENTAL AREA
10 FEET
MU-6090

Sec. III, Fig. 2

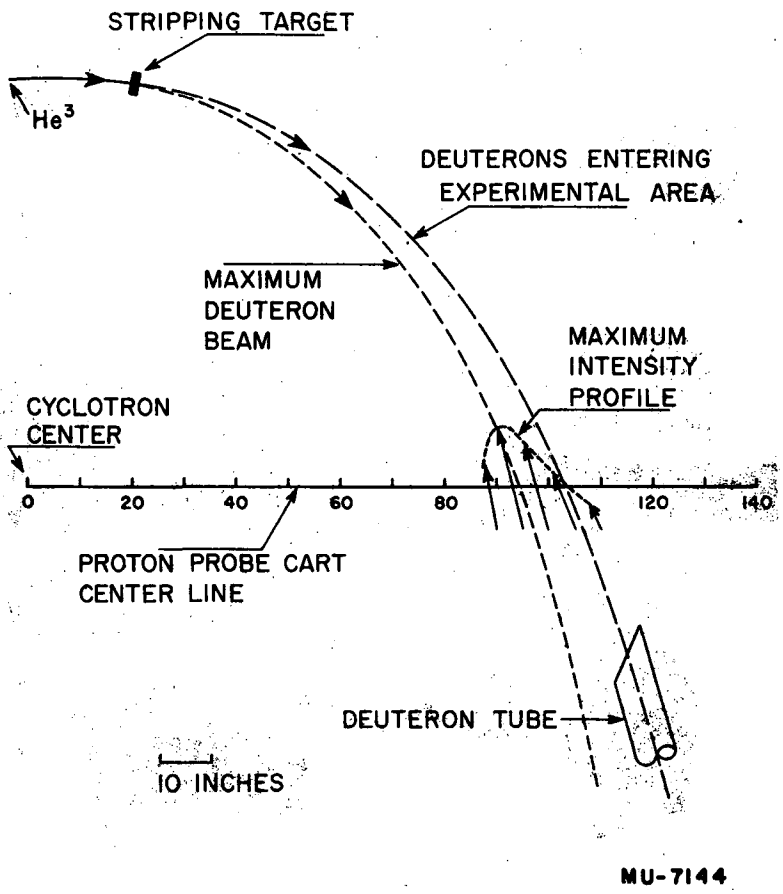
STRIPPING TARGET
He3
DEUTERONS ENTERING EXPERIMENTAL AREA
MAXIMUM DEUTERON BEAM
MAXIMUM INTENSITY PROFILE
CYCLOTRON CENTER
0
20
40
60
80
120
140
PROTON PROBE CART CENTER LINE
DEUTERON TUBE
10 INCHES
MU-7144

Sec. III, Fig. 3

Energy Spectrum of Stripped Deuterons

Theoretical study of the energy spectrum of the deuterons stripped from the 493-Mev He^3 ions indicated a half-width of about 50 Mev. No experimental check is at present available on this prediction, but it is possible to calculate the energy distribution of the deuterons after emergence from the focus magnet and the deuteron tube, by means of the attenuation curves of the deuterons in uranium. The deuterons obtained from stripping of the 4 percent He^3 beam were allowed to traverse various thicknesses of uranium absorber and were then captured in the copper block of a Faraday cage constructed to measure currents lower than 10^{-15} ampere. The beam incident upon the absorber was monitored meanwhile by means of a parallel-plate ionization chamber.

The experimental attenuation curve is shown in Fig. 4. We have shown from a study of the attenuation of monoenergetic 190-Mev deuterons that the attenuation curve can be explained quite satisfactorily, at this energy, by means of only three cross sections, all essentially independent of particle energy:

(1) attenuation of the deuterons with a total inelastic cross section σ_1 of 3.75 barns,

(2) stripping of the deuterons with a total stripping cross section σ_2 of 1.75 barns,

(3) attenuation of the stripped protons with an effective attenuation cross section σ_3 of 2.0 barns.

This scheme thus assumes no "knock-out" particles from deuteron collisions with uranium nuclei.

It has been shown both experimentally and theoretically that the logarithmic attenuation curve for monoenergetic deuterons consists of two linear portions, the first of slope $-\sigma_3$ out to half the range, and the second of slope $(\sigma_3 - 2\sigma_1)$ from there on, with some rounding near the end of the range due to range straggling and the variation with energy of the various cross sections. To explain the attenuation curve for the He^3-stripped deuterons, an energy spectrum is calculated by assuming different fractions of the beam in various energy intervals, calculating the attenuation curve for each energy interval, and combining the several curves for best fit with the experimental curve.

The calculated energy spectrum is shown in Fig. 5. The significant features of the curve are:

(a) the sharp cutoff at energies above 340 Mev,

(b) the main bulk of the spectrum, centered at 320 Mev, and

(c) the small low-energy tail.

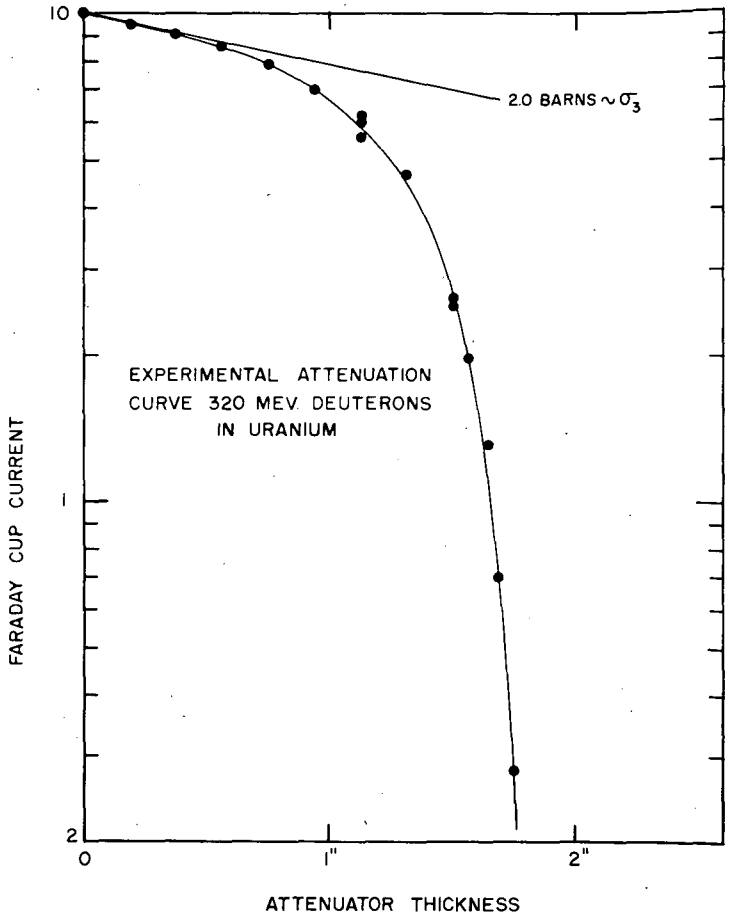

Sec. III, Fig. 4 Experimental attenuation curve for 320-Mev deuterons in uranium.

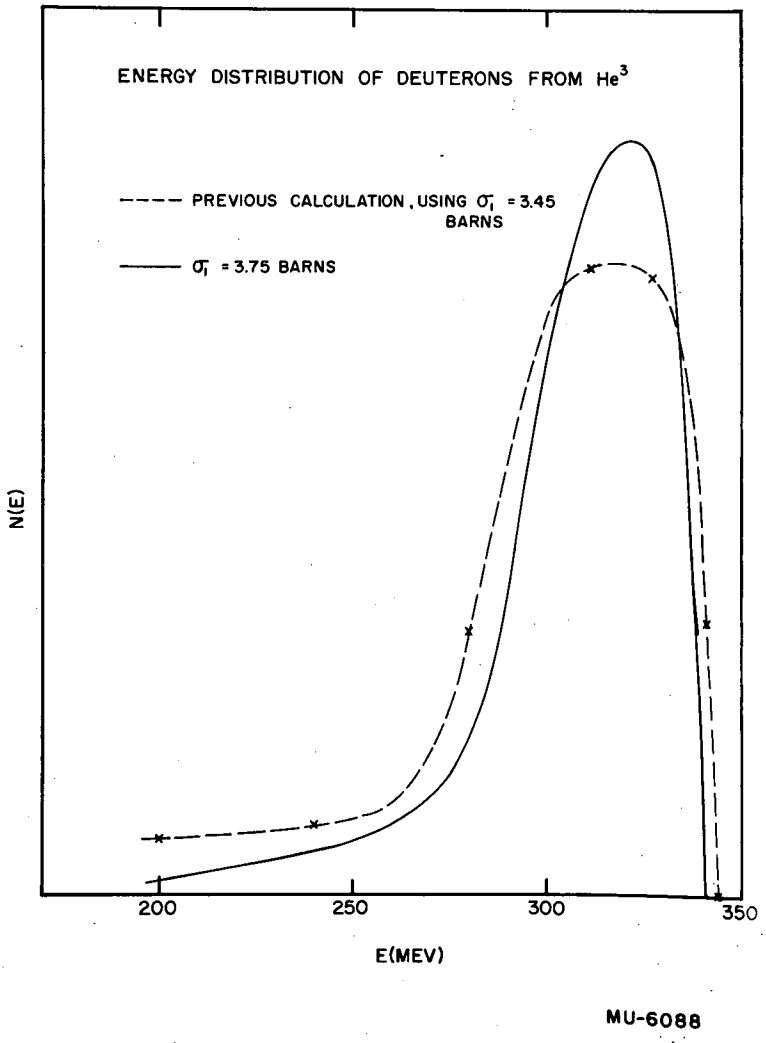

Sec. III, Fig. 5 Energy distribution of deuterons from He^3.

The shape of the spectrum is insensitive to the values of σ_2 and σ_3, but the main features of the spectrum seem to be fairly well established. A previous calculation of the energy spectrum, based on $\sigma_1 = 3.45$ barns, is also shown in Fig. 5, and reveals the same general shape, with the important differences that

(a) the new calculation leads to a considerably narrower spectrum, and

(b) the low-energy tail is greatly reduced by the new value of σ_1.

A further experimental check on the shape of the energy spectrum of the stripped deuterons emerging into the cave is provided by means of the time-of-flight spectrometer, which consists essentially of two scintillation counters placed in the beam and separated by a known variable distance. A preliminary run with this equipment has confirmed the narrow spectrum and the absence of the low-energy tail, although the position of the peak energy is still somewhat uncertain.

Further details are given in UCRL-2319 2nd Rev.

Inelastic Cross-Section Measurements

Wallace Birnbaum, Walter E. Crandall and Larry Schecter (CRD)
and George P. Millburn (UCRL)

The total inelastic cross sections of high-energy particles for several elements have been determined by an attenuation technique. Much of the emphasis has been concentrated on the behavior of 190-Mev deuterons while traversing an absorbing medium, but the experimental technique has been extended to include the attenuation of 340-Mev protons, 490-Mev He^3 particles, and 380-Mev alpha particles. The latter cross sections have been determined with somewhat less precision because of the limitations of the experimental method and consequent uncertainties in the interpretation of the data.

These attenuation cross sections are fundamental in the general understanding of nuclear processes. The comparison of the respective inelastic cross sections gives further information regarding the structure of the nucleus and the effects of nuclear transparency. Furthermore, from the deuteron data, stripping cross sections can be determined for the different elements serving as attenuators.

A complete description of the experimental method and the interpretation of the cross sections in terms of various nuclear models will be issued as a separate report (LRL-85). A summary of the measured inelastic cross sections is given in Table I. Included in this table are measurements of the inelastic cross section previously published by other experimental groups, which are pertinent to the theoretical interpretation of the data.

Figures 6, 7, and 8 clearly show that the inelastic cross sections for a bombarding particle of n nucleons can be written

$$\sigma_n = \pi(a_n A^{1/3} + r_n')^2 .$$

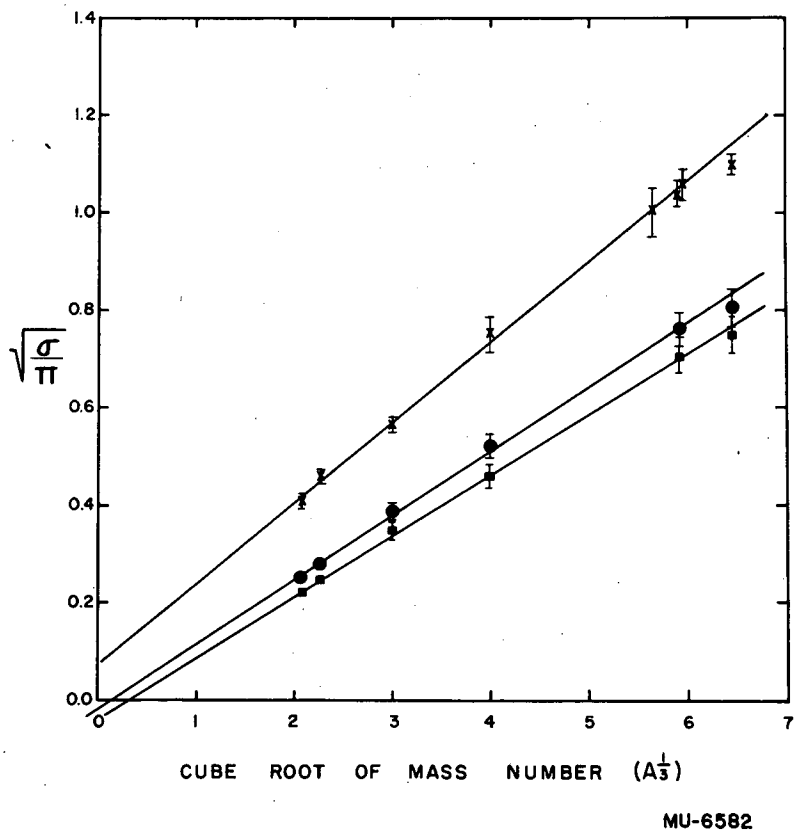

Sec. III, Fig. 6 Plot of $\sqrt{\sigma/\pi}$ vs. $A^{1/3}$ for 80-Mev (●) and 300-Mev (■) neutrons, and 160-Mev (x) deuterons.

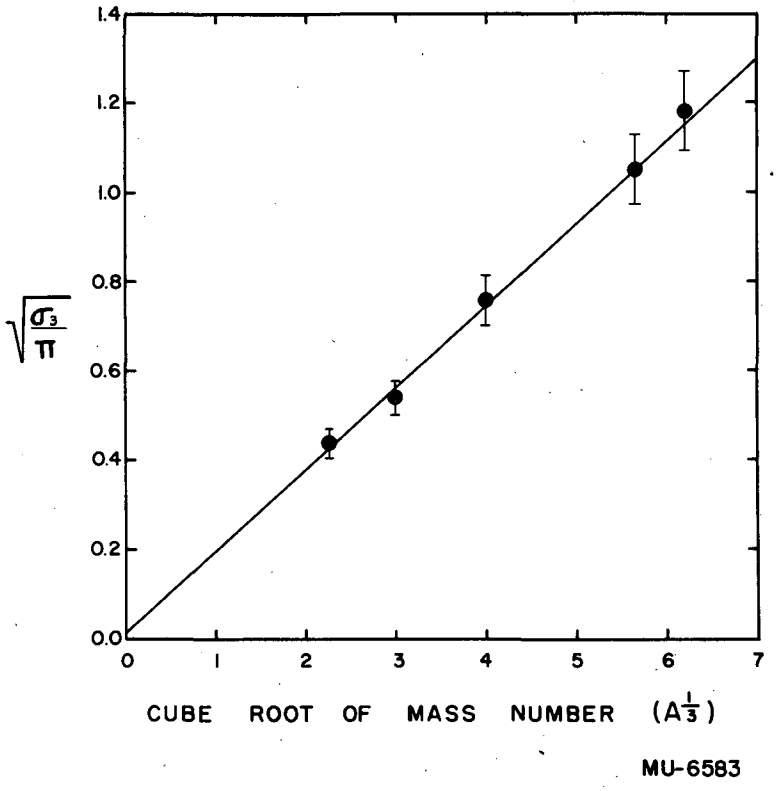

Sec. III, Fig. 7 Plot of $\sqrt{\sigma_3/\pi}$ vs. $A^{1/3}$ for 315-Mev He^3 particles.

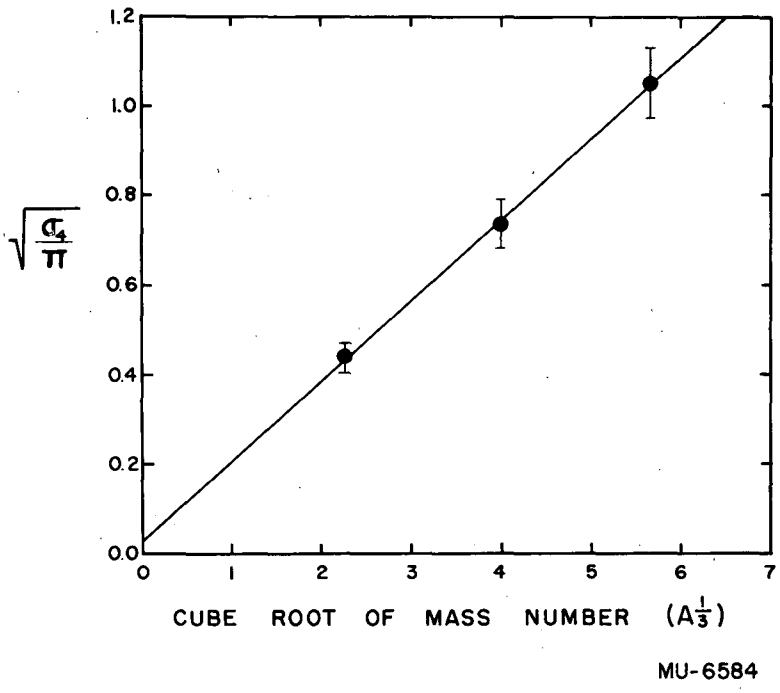

Sec. III, Fig. 8 Plot of $\sqrt{\sigma_4/\pi}$ vs. $A^{1/3}$ for 240-Mev alpha particles.

Table I

Inelastic Cross Sections for High-Energy Particles

A. Neutrons

	84 Mev[4] (Upper Limits)	95 Mev[1] (Lower Limits)	270 Mev[2] (Lower Limits)	300 Mev[3]
Carbon	---	0.222 ± 0.009	0.145 ± 0.006	0.203 ± 0.033
Aluminum	0.50 ± 0.05	0.418 ± 0.017	---	0.390 ± 0.023
Copper	0.91 ± 0.05	0.782 ± 0.013	0.573 ± 0.024	0.755 ± 0.033
Lead	1.85 ± 0.18	1.75 ± 0.05	1.42 ± 0.06	1.72 ± 0.08

B. Protons (10 percent errors)

	350 Mev[5]	240 Mev[5]	185 Mev[5]	290 Mev
Beryllium	0.151	0.169	0.172	---
Carbon	0.187	0.202	0.204	0.199
Aluminum	0.334	0.383	0.408	0.416
Copper	0.608	0.667	0.746	0.717
Lead	1.48	1.57	1.55	---
Uranium	1.60	1.77	1.90	1.85 2.03 (230 Mev)

C. Deuterons, He^3 and Alpha Particles

	160 Mev H^2	315 Mev He^3	240 Mev He^4
Beryllium	0.512 ± 0.025	---	---
Carbon	0.667 ± 0.033	0.60 ± 0.10	0.64 ± 0.10
Aluminum	0.996 ± 0.050	0.91 ± 0.15	---
Copper	1.76 ± 0.17	1.8 ± 0.3	1.8 ± 0.3
Tantalum	3.13 ± 0.30	3.5 ± 0.5	3.5 ± 0.5
Lead	3.44 ± 0.17	---	---
Bismuth	3.55 ± 0.18	---	---
Uranium	3.81 ± 0.15	4.4 ± 0.7	---

1 J. DeJuren and N. Knable, Phys. Rev. 77, 606 (1950).
2 J. DeJuren, Phys. Rev. 80, 27 (1950).
3 William P. Ball, Nuclear Scattering of 300-Mev Neutrons, Ph. D. Thesis, University of California Radiation Laboratory, Report No. UCRL-1938.
4 A. Bratenahl et al, Phys. Rev. 77, 597 (1950).
5 A. J. Kirschbaum and D. A. Hicks, CRD report MTA-28.

The parameters a_n and r_n' were determined by the method of least squares and are listed in Table II, while A is the mass number of the struck nucleus. This equation is open to certain interpretations. If one assumes that $r = a_n A^{1/3}$ is related to the nuclear radius, then the functional dependence of a_n on the bombarding particle must be due to nuclear transparency. To allow for transparency the above expression can be rewritten as

$$\sigma_n = \pi(A_o A^{1/3} + r_n)^2(1 - \tau_n) ,$$

where now the radius of the nucleus is given by $r = a_o A^{1/3}$, and the average transparency by τ_n. Furthermore, if the bombarding particle is treated as a loosely coupled assembly of nucleons, the transparency factor may be expressed as $\tau_n = \tau^n$ and the cross section expressed as

$$\sigma_n = \pi(a_o A^{1/3} + r_n)^2(1 - \tau^n) .$$

This expression fits the experimental data with fewer independent parameters. The values of these parameters from a least-square fit of the data are

$$a_o = (2.0 \pm 0.3) \times 10^{-13} \text{ cm}$$

$$\tau = (0.55 \pm 0.12) .$$

As already stated, a more comprehensive discussion of the experiment is made in LRL-85.

Table II

Slopes and Intercepts for Straight-Line Fits of Inelastic Cross Sections

Particle	Mean Energy (Mev)	Slope $\times 10^{13}$ (cm)	Intercept $\times 10^{13}$ (cm)
Neutron	80	1.37 ± 0.07	-0.33 ± 0.20
Neutron	300	1.26 ± 0.06	-0.41 ± 0.18
Deuteron	160	1.68 ± 0.04	0.64 ± 0.08
He^3	315	1.92 ± 0.18	-0.12 ± 0.61
Alpha	240	1.84 ± 0.42	0.35 ± 1.1

Time-of-flight Measurements of the 320-Mev Deuteron Beam

Larry Schecter and Donald A. Hicks (CRD)

The resolving time of the coincidence circuit used in the time-of-flight apparatus was measured to be about 10^{-9} seconds full width at half maximum, using an artificial pulse generator (mercury-relay delay line). The apparatus was calibrated against the time of flight of the 190-Mev (nominal) deuterons from the 184-inch cyclotron, the energy variation of the deuterons being less than ± 2 percent. Since deuterons are emitted over all of the beam pulse duration (about 40 microseconds), some ambiguity might result from detection of two different deuterons in the detector scintillator. To minimize this possibility, the cyclotron beam intensity was reduced by severe collimation and reduction of gas pressure until only about one particle per beam pulse was detected by the monitor counter in the experimental area.

The cable lengths and counter separations having been determined from the known velocity of the 190-Mev deuterons, the 320-Mev deuteron beam was then run and the coincidence rate as a function of counter separation was determined for known cable lengths. From this, it is possible to "unfold" the velocity spectrum (and hence the energy spectrum) of the high-energy deuterons. The results were in agreement with those obtained by range-attenuation methods (UCRL-2285) as regards the width of the spectrum (half width about 40 Mev) and the absence of an appreciable low-energy tail, but the position of the peak energy as determined by the time-of-flight method turned out somewhat lower (~300 Mev) than that given in UCRL-2285. Since only one run was made with the time-of-flight equipment, this is not considered a serious discrepancy.

High-Energy Yield Calculations

John Ise, Jr.

Since the calculations of total neutron yield vs. deuteron energy made in UCRL-1389, the values of the significant cross sections have changed considerably (LRL-85, UCRL-2285, -2319). In particular, the stripping cross section, which determines the yield from secondary multiplication in the secondary target, has been raised from 1 barn to 1.8 barns, and on the basis of attenuation cross-section measurements described in LRL-85 this can be considered as approximately constant over a wide energy range. Similarly, the total inelastic cross section for deuterons has been changed to 3.8 barns, this also being approximately a good constant.

The experimental values of total neutron yield were higher by about 25 percent than those calculated in UCRL-951, but the slopes of the yield-vs.-energy curves agreed reasonably well.

The new calculations give a yield of 3.3 neutrons per deuteron at 190 Mev, and about 10.5 at 320 Mev, assuming that the yield of tertiary neutrons from stripped neutrons goes linearly as the stripped-neutron energy. This assumption is possibly in error, since there are some indications of a saturation effect in σ_{1n} with protons, but recent measurements indicate that

this saturation is considerably less than formerly believed. In any event, any possible saturation yield (from stripped neutrons) is only about 20 percent of the primary yield (from direct deuteron interactions) at 320 Mev, and the saturation effect in σ_{1n} affects only the secondary yield.

The new calculations therefore agree almost precisely at 190 Mev with the experimental value, and are perhaps 10 percent high at 320 Mev, but this is not considered unreasonable in view of the accuracy of these calculations and the uncertainties in the experimental data.

N-P Recoil Experiment

Robert Main (CRD) and Marian N. Whitehead (UCRL)

In order to make a complete analysis of the production of neutrons by high-energy deuterons incident upon various target materials it is desirable to separate the various competing processes and study them individually. To this end it has been suggested that the production of neutrons by high-energy neutrons be investigated, utilizing the neutron beam from the 184-inch Berkeley cyclotron in an $MnSO_4$ tank experiment.

To carry out this experiment it is necessary to determine, in some manner, the intensity and energy spectrum of the neutron beam. Two methods for making these measurements have been investigated by this group. The first, a time-of-flight spectrometer, was abandoned in favor of the method here discussed, owing to the stringent fast-coincidence requirements inherent at the neutron energies to be encountered.

The technique decided upon is as follows: A polyethylene (carbon) target is placed in the neutron beam. Recoil protons from the target pass into a three-counter telescope. If an absorber is placed between the first two counters some of the protons stop in the second counter. The coincidence 1-2 anti-3 thus designates a proton, the energy of which can be calculated from its known range in the counters and absorber with the energy interval determined by the stopping power of the second counter. If the absorber thickness is varied the relative number of protons of any energy can be found. In addition, if the counter system is efficient, and if the n-p cross section is known for the energies involved, the energy spectrum of the neutron beam can be determined.

The operation of the telescope as described involves rather strict requirements. First, since the tank experiment must be run with high neutron flux, considerable background is to be expected, necessitating relatively fast coincidence. Second, since the measurement involves the subtraction of two nearly equal large numbers, the counter system must be perfectly efficient.

Plastic scintillators with 1P21 (RCA) photomultiplier tubes were selected for the telescope counter because of the facility of construction. The coincidence circuit is of the bridge type designed for pulses of 0.10 to 10 volts, of 2×10^{-8} second duration. The requirement of 100 percent efficiency in the counter system demands some method of limiting the photomultiplier so that all protons, independent of the amount of light they produce in the scintillators, give pulses lying within the range accepted by the coincidence circuits. Unsuccessful attempts to accomplish this limiting action by conventional methods led to the development of a circuit which would make the photomultiplier tube self-limiting.

Two cyclotron runs using this equipment were made during the month of October. The first was a preliminary run to check out the electronics. It showed by photomultiplier high-voltage plateaus, which were perfectly flat for several hundred volts, that the counter and coincidence circuits were counting all particles. However, slight defects in the telescope geometry were revealed and the energy resolution was found to be insufficient. During the second run it was not possible to obtain perfect plateaus, but good energy resolution was indicated and the geometry of the system was checked out.

A third run was made in November, when good plateaus were again obtained. A more complete energy spectrum of the 90-Mev neutron beam from a 1/2-inch beryllium target was found. The results appear to be in good agreement with the expected spectrum. An appreciable part of the run was taken up by searching for voltage and discriminator plateaus, etc. It is expected that, with a few modifications of the equipment, good absolute values of the neutron flux can be obtained. Measurements can then be made on the higher-energy neutron beams from 340-Mev protons and 500-Mev He^3 particles.

Liquid-Scintillator Neutron Detector

John Ise, Jr. and Robert V. Pyle

Some considerations concerning the construction of a large-volume liquid-scintillation neutron detector of high efficiency were mentioned in UCRL-2318. Briefly, the proposed design was a cylindrical steel tank 30 inches in diameter and 30 inches high with 90 end-window photomultiplier tubes viewing the scintillator solution. We proposed to load the solution with a cadmium compound to capture neutrons thermalized in the liquid and detect the γ-rays subsequently given off.

At this point we learned that a group at Los Alamos had already built and operated a device of almost identical properties, and we have been able to make use of their experience, in particular that which concerns the optimum composition and possible poisoning of the scintillator solution.

In the past six months the tank has been fabricated, and further research on the design has been carried out. All necessary components are now on hand and the final assembly has begun. Certain aspects are discussed in more detail in the following paragraphs.

The Tank. The tank is a circular cylinder of 1/4-inch mild steel 30 inches in diameter and 30 inches high, with a removable lid. An 8-inch-diameter tube can be inserted through the center of the tank so that targets can be bombarded with particles from the various accelerators. Ninety inserts are arc-welded into the curved surface of the cylinder, and in these are clamped 1/4-inch-thick pyrex glass disks, 3 inches in diameter, the liquid seal being made with neoprene O-rings that have been soaked in benzene and toluene to remove compounds that would discolor the scintillator solution. Iron sleeves containing the photomultiplier tubes bolt onto the inserts and films of mineral oil make the optical seals between the pyrex windows and the photomultiplier tubes. Mild steel has been used in the construction to shield the photomultipliers from the stray magnetic field of the cyclotron.

The inner surface of the tank must be coated with a material which (a) is highly reflecting and (b) will not affect the scintillator. We have investigated porcelain and found it to have desirable properties but to be expensive and difficult to apply. A paint made of TiO_2 in sodium silicate (suggested by the Los Alamos group) shows a tendency to scale off and discolor. We have recently obtained an experimental epon-base paint which appears very satisfactory. Should any deterioration show up we will coat it with the TiO_2 and sodium silicate mixture.

Scintillator Solution. Techniques are constantly improving, but a satisfactory mixture which will be used for the initial filling consists of terphenyl and α-NPO in toluene, loaded with cadmium propionate dissolved in methanol. Solutions of this type have been tested for emission and absorption of light in the visible region. The absorption length is many tens of meters. To avoid contamination, the material will be stored in stainless steel drums and moved through tygon tubing by gravity or nitrogen pressure.

Photomultiplier Tubes. A device to age and test the photomultiplier tubes (Dumont type 6292) has been constructed, and the product gain times cathode efficiency is made the same for all tubes by adjusting a resistance in the voltage-divider chains on the tube bases.

Theoretical Nuclear Studies

Warren Heckrotte

Nuclear Evaporation and Fission

The relation between fission and neutron evaporation at high excitation energies has been examined on the basis of the available data.

The conclusions, which are rather limited, have been written up in UCRL-2184 revised.

Simple formulas for the results of the Monte Carlo calculation on neutron evaporation have been obtained. These are also contained in UCRL-2184 revised.

Inelastic Proton Cross Sections

The cross sections for the formation of U^{237} and Pa^{237} from the 340-Mev proton bombardment of U^{238} are about 0.25 barn and about 0.002 barn or less respectively (Batzel and Lindner, private communication). If the production of these elements proceeded by knock-on reactions, leaving the product nucleus in a bound state, one would expect that the cross sections would be comparable. The principal differences would be in p-p and p-n cross sections and in the number of protons and neutrons in the U^{238} nucleus. These factors, however, lead to a cross section for U^{237} only 2 or 3 times as great as for Pa^{237}. This suggests that (1) the knock-on reactions leave the residual nucleus with enough excitation energy to evaporate one or more neutrons, and (2) the disparity in the above cross section is due to another cause.

This disparity can be explained on the following assumption: there is a large cross section for the incident proton to suffer an inelastic collision involving small energy losses. If between 6 to 12 Mev is transferred to U^{238}, then, because the proton emission is inhibited by the Coulomb barrier, the U^{238} will emit one neutron leading to U^{237}. Very little Pa^{237} can be formed this way, and the disparity is explained. The fission width at these energies is about 1/3 of the neutron width, so that the cross section for the transfer of from 6 to 12 Mev excitation energy to the U^{238} nucleus by 340-Mev protons is about $(4/3)0.25 \simeq 0.33$ barn.

This explanation correlates with other experimental material also. Kirschbaum has measured the inelastic cross section for 300-Mev protons and found that the mean free path in nuclear matter increases from 4×10^{-13} cm on C^{12} to 8×10^{-13} cm in U^{238}. In measuring these inelastic cross sections, though, he does not count as inelastically scattered those protons which suffer an energy loss of only 20 or 30 Mev or less. If now one includes the 0.33 barn for energy losses between 6 to 12 Mev, the mean free path is reduced to 6×10^{-13}. It seems reasonable to expect that if the cross section represented in the parts of the low-energy interval other than 6 to 12 Mev are included, the mean free path in U^{238} would be reduced to about the value for C^{12}. This implies, of course, that low-energy transfers are more probable in heavy nuclei than in the light nuclei.

The formal aspects of this problem are being examined.

Deuteron Attenuation and the Size of the Nucleus

The results of the deuteron-attenuation cross-section measurements of Birnbaum, Crandall, Schecter, and Millburn are summarized by the following formula:

$$\sigma = \pi(1.68\ A^{1/3} + 0.64)^2 \times 10^{-22}\ \text{cm}^2$$

where σ is the deuteron-attenuation cross section and A is the mass number of the target nucleus.

Using the classical picture of deuteron stripping introduced by Serber and assuming that, if either or both particles of the deuteron interact with a target nucleus, the deuteron is broken up, the attenuation cross section is given by

$$\sigma = \pi R^2 + \frac{\pi}{2}\rho r$$

where $R = r_o A^{1/3} \times 10^{-13}$ cm is the nuclear radius and $\rho \simeq 3 \times 10^{-13}$ is the deuteron radius. This can be rewritten as

$$\sigma = \pi\left(R + \frac{\rho}{4}\right)^2 - \frac{\pi\rho^2}{16}.$$

The term $\frac{\pi\rho^2}{16} \simeq 0.02$ barn. Neglecting this, one has

$$\sigma = \pi\left(R + \frac{\rho}{4}\right)^2 = \pi(r_o A^{1/3} + 0.75)^2 \times 10^{-26}.$$

The experimental results indicate that $r_o \simeq 1.65$, which is considerably larger than the value that is commonly accepted.

This larger value of the nuclear radius can be reconciled with the usual idea of a smaller nuclear radius if it is assumed that the nucleus is not of uniform density but is smeared out to some extent. The outer fringes of this smeared-out nucleus can still break up the deuteron, yielding a larger nuclear radius even though the bulk of the nuclear matter is contained in a considerably smaller volume.

To check these ideas, calculations are being made to see if the 90-Mev total neutron cross sections can be fit by a smeared-out density distribution. The density distribution has been taken to be proportional to $[1 - (r^2/R_o^2)]$ where $r < R_o$. This choice was made for the sake of simplicity in the numerical work. The tentative result of these calculations, which are now in progress, is that the data can be fit with an $R_o \simeq 1.6\ A^{1/3}$. Considering the ad hoc nature of the density distribution, this is a good fit with the result of the deuteron experiment.